Metal micro drilling combining high power femtosecond laser and trepanning head

R. Kling *[a], M. Dijoux [a], L. Romoli [b], F. Tantussi [c], J. Sanabria [d], E. Mottay [d]

[a] Alphanov, 351 Cours de la Libération, bâtiment A11, 33405 Talence, France
[b] Dep. of Industrial and Civil Engineering, University of Pisa Largo Lucio Lazzarino Pisa, Italy
[c] Department of Physics, University of Pisa Largo Bruno Pontecorvo 3 Pisa, Italy
[d] Amplitude Systemes, 11 avenue de Canteranne, Cité de la Photonique, 33600 Pessac, France

ABSTRACT

Trepanning heads are well known to be efficient in high aspect drilling and to provide a precise control of the hole geometry. Secondly, femtosecond lasers enable to minimize the heat effects and the recast layer on sidewalls but are typically used on thin sheet. The combination of both present a high potential for industrial applications such as injector or cooling holes where the bore sidewall topology has a major influence on the dynamics of the gas flow. In this paper we present results using this combination. The effect of pulse energy, repetition rate and revolution speed of the head on both geometry and roughness are discussed. The quality of the sidewall is checked by roughness measurement and by metallographic analysis (SEM; chemical etching, micro hardness).

Keywords: trepanning, drilling, roughness, tolerance, conicity, taper

* E-mail: rainer.kling@alphanov.com; www.alphanov.com

1. INTRODUCTION

1.1 Motivation

Current drilling and machining processes for fine features and deep holes are mainly based on EDM, micro electro discharge machining. This is a process to remove any conductive material by using electrical discharge; EDM uses very short electrical pulses with high energy discharge. Looking at fuel injectors where the blanks are called ‘seats’ the hole diameter is the main parameter that controls the seat static flow. On an EDM machine the hole diameter is the same for all holes and it is, first of all, determined by electrode diameter one of the main design limitations on the process. Although an EDM machine has the possibility to introduce small modifications, for flow adjustment, on holes’ diameters by changing the run-out of the electrode, it is in a small range (10-60 µm).

EDM technology has the advantage to be a robust and well known drilling process, but it has some drawbacks regarding productivity: the hole erosion and machining times are long (15-60 s) in order to obtain the required final quality in terms of static flow and hole shape (circularity, cylindrical shape, no burrs and small heat affected zone, sharp edges). In addition costs for maintenance are high which makes EDM an expensive process for daily production. On other aspect to improve over EDM technology is the achieved surface roughness which is in the range of 300nm on the sidewalls depending on the discharge current [30]. Therefore EDM drilling requires a compromise between drilling speed and surface quality.

For passenger cars there is continuous increase of emissions restrictions. This pushes future drilling technologies for fuel injector nozzles toward the possibility to have completely flexible spray shapes. In term of seat characteristics this means individual diameter, length, holes shape, for optimized and fully customizable spray distribution and mixture formation. EDM technology couldn’t offer the flexibility to provide 3D shapes. The existing fuel injections nozzles are based on 100-140 µm holes. For more effective atomization and fuel combustion and reduction of emissions, smaller holes are needed. The current EDM technology is struggling with smaller holes as the electrode lifetime is shorter and the cost is significantly higher. Nanosecond pulsed lasers cannot meet the quality requirement. Picosecond lasers have

Laser-based Micro- and Nanopackaging and Assembly VII, edited by
Udo Klotzbach, Yongfeng Lu, Kunihiko Washio, Proc. of SPIE Vol. 8608, 86080F
 · doi: 10.1117/12.2002083

demonstrated high quality drilling, but the material removal rate has been too low due to low average power in the initial phase.

In the last 20 years, there have been investigations into different laser sources, with different drilling/machining strategies. Simple hole configurations have been produced and compared with EDM reference: by first analysis, ultrashort lasers, with a trepanning optic, is a solution which leads to higher process speed and higher quality at the same time. Moreover, this technology provides, with respect to EDM, interesting advantages: low tooling cost (e.g. no wearing parts), possibility to change hole diameter and shape without any changeover, and hole by hole on one seat, possibility to modify internal hole shape and its conicity, control on internal hole surface roughness. However the impact of a HAZ in terms of creating stress weakness, surface warping or cratering around holes has deterred the readiness of laser systems for practical production. The combination of Laser drilling with post EDM machining has been proposed [19] but not applied in industrial applications, yet.

1.2 Need for ultrashort pulses

Laser ablation is the process of removing material from a surface by laser beam irradiation. Short pulse laser ablation is advantageous since the material can be heated up to the temperature of vaporization in a very short time. This means that the energy does not have time to spread into the deeper parts of the material and thereby the energy is localized where it is needed.

Vast resources have been invested in the development of new laser systems and specifications as for instance stability and power have increased immensely. For industrial applications stability is obviously a necessity but also the average power must be high since production time is of great concern. For laser surface structuring to be an industrially applicable technique, material removal rates of the order of 1 mm^3/s must be realized.

The growing application of laser systems generating ultrashort laser pulses in the field of material processing is based on the advantages that they offer compared with nanosecond pulses. Experiments on micro-machining of a wide range of materials by ultrashort pulses [1-4] have shown that they ensure negligible heat diffusion into the material and absence of plasma during the laser pulse. As a consequence, the ablation threshold decreases (by one order of magnitude in some cases [4]) compared with nanosecond pulses, so that precise sub-micron machining becomes possible with minimization of the heat affected zone. Indeed, application of ultrashort laser pulses proved to be particularly suitable for the treatment of materials having high heat conductivity, e.g. metals and semiconductors.

Recent studies [5-14] have shown that the process of interaction of ultrashort laser pulses with matter is very complicated and is strongly influenced by the parameters of the laser radiation, the properties of the material, the processing conditions, and the environment. Experimental works on laser ablation of metals [5-7] have indicated that, in contrast to the case with nanosecond pulses, the electron thermal diffusion can play an important role in the process of dissipation of the absorbed energy and the properties of the electron–phonon coupling are important for pico- and femtosecond laser induced damage. It has also been shown that the process of ablation can be accompanied by a fast nonlinear phase transition, such as melting and amorphization [11], and formation of three dimensional structures within the ablation region [9,10,13] which affect the ablation rate.

Drilling by high laser intensities (10^{15} W/cm^2) [15] has shown that some of the advantages of using ultrashort pulses can be lost. Laser ablation with such intensities can be accompanied by a considerable amount of molten material and high temperature gradients, leading to stresses, which can cause deformation, dislocation, or crack formation in the material.

The interaction between metals and ultra-short laser pulses is still not fully understood: the presence of different processes in ultrashort laser ablation makes its theoretical modeling difficult. However, some recent theoretical investigations [8, 15-17], based mostly on molecular dynamics simulations, two temperature heat diffusion models, and fluid dynamics models, have shown that some of the main features of the process could be described and explained.

1.3 Fundamental considerations on heat effects

The material properties in the interaction zone are changed due to laser ablation. Many parameters have an influence on that e.g. wavelength and polarization determining the absorption behavior. However for the heat effects inside the material predominantly the pulse duration and peak power alter the thermal load which leads to mechanical stress and eventually to defects like micro cracks. Therefore these two parameters are discussing in the following to some larger extend.

Temporal distribution of energy can greatly influence the interaction between the laser and material. The heat affected zone (HAZ) can be controlled by changing the pulse duration. The effect of pulse duration becomes more prominent as it changes from nanosecond to picosecond and femtosecond. HAZ zone could be decreased to almost zero by these ultrashort pulsed lasers.

According to [18, 21] the effect of pulse duration on HAZ can be explained by comparing the pulse duration T_l with electron relaxation/cooling time T_{el} (in the order of 1 picosecond) and the time for electron to transfer energy to lattice T_{ion} (lattice heating time). T_{el} and T_l are proportional to the heat capacity and since electrons have a much smaller heat capacity than the lattice therefore $T_{el} << T_{ion}$.

There arise three different cases for T_l in three different ranges.

- For pulses longer than 1 millisecond (T_l > 1ms >> T_{ion} >> T_{el}) or continuous wave lasers, there is sufficient time for the electrons to relax and transfer energy to the lattice. The lattice can reach equilibrium and there is conduction of heat from the beam spot area to the material. Melting takes place and small percentage of the material is vaporized. Material removal mechanism is dominated by melt ejection supported by the assist gas and the vapor recoil pressure. Therefore spatter/recast and HAZ can be formed upon cooling and solidification.

- For pulse duration in nano scale range T_l > 1ns >> T_{ion} >> T_{el}) the electrons absorb energy and have sufficient time to transfer the energy to the lattice. There is thermal equilibrium between electrons and lattice. The material is first melted and if the incident energy is high enough then evaporation (and plasma formation) occurs. Fundamentally, there is slight melting followed by quick evaporation. In this case, the material removal mechanism is dominated by vaporization. However, some melted layer still exists and thus a smaller HAZ is witnessed as compared to continuous or long pulsed lasers.

- For pulses in the femtosecond range (T_l << T_{el} << T_{ion}) the pulse duration is much shorter than the time required for electrons to relax and transfer energy to the lattice. Electrons are heated instantly and in about 1 picosecond they transfer energy to the positive ions. If the energy is high enough, which is common for ultra-short pulses, the ions get energy which is high enough to break the lattice bonding. Direct solid vapor transition occurs because of insufficient time to transfer energy to the neighboring lattice ions. Heat conduction is thus negligible and HAZ is minimal. Melt free ablation occurs because of the ultra-short pulse and high pulse energy. Almost all materials can be processed at this time scale because absorptivity is less sensitive to the laser wavelength due to avalanche ionization and multiphoton absorption.

The second major influence on HAZ is the peak power density on the workpiece determined by the pulse energy divided by the pulse duration and focus spot size. Again, the interaction regimes can be classified in major sections representing the dominating ablation regimes.

- At low power densities with continuous or long laser pulses irradiances below 10 MW/cm² can be obtained. Due to heat conduction and long interaction times melt formation is the dominant ablation mechanism. Here melt pool dynamics influenced by assisting gas flows is the major parameter which determines the hole geometry and often accompanied by striation effects. Striation on side walls is also an intensely investigated phenomenon in laser cutting as it impairs the quality in sheet metal cutting and is difficult to suppress.

- Between 10 and 100 MW/cm² the incident power density leads to a fast transition from the melt to vapor phase reducing the layer of molten material and therefore the HAZ. However side effects like spatter formation and recast layers are still present which make it necessary to have post processing like wet chemical etching to meeting the high quality requirements.

- In the power density range above 100 MW/cm² the light interaction with matter cannot be described by means of statistical parameters like common temperature as the gradients in energy are too step to form an equilibrium (LTE condition) [7]. Energy transfer can only be described in a fair approximation by the two temperature model introduced by Anisimov in 1974 [20]. Due to multiphoton absorption and rapidly increasing electron density almost any material exhibits optical properties like metals with strong absorption and high mobility of electrons [21]. Therefore the direct transition from solid to vapor phase is followed by intense plasma formation. Different models have been developed to describe this behavior like superheated ejection, phase explosion and Coulomb explosion, just to name a few see e.g. [8]. This regime is accompanied by several side effects which can reduce both process efficiency and quality. Inside the hole the plasma can either improve

surface quality due to ion etching or create defects like micro cracks due to thermal load of the expanding plasma. Therefore the pulse energy and repetition rate need to be chosen carefully to have control of these secondary mechanisms. In recent publications the most accurate control of the hole geometry has been demonstrated in this regime [22].

Therefore in the current paper we investigate the combination of a high average power ultrashort pulsed laser with a trepanning head for high quality hole geometry and in particular the sidewall roughness.

2. EXPERIMENTAL

2.1 Drilling Setup

In our experiments of stainless steel drilling, we used a trepanning head, combined with a femtosecond laser. We used a new generation of femtosecond Yb-doped fiber laser (Tangerine from AMPLITUDE SYSTEMES), offering the highest average power which is commercially available today from this kind of laser. It generates pulses with duration below 500fs and pulse energy up to 150µJ at a laser wavelength of 1030nm. Repetition rates can be selected up to 2 Mhz in standard configuration, but in the present set-up it was limited to 100kHz due to the high pulse energy.

Figure 1: AMPLITUDE SYSTEMES Tangerine fiber laser

This laser has been combined with a SHG/THG module, which allowed us to generate a femtosecond laser wavelength of 515nm with 80µJ of pulse energy at 100 kHz. The pulse energy was controlled with an attenuation system composed by λ/2 plate and a polarizer cube in order to maintain a constant pulse width and constant beam properties for all trials. We also put a λ/4 plate to transform the linear polarization into circular polarization, in order to avoid Fresnel absorption effects due to different polarization orientation on the sidewalls. Arranging a circular symmetry in all laser parameters the best conditions for a good roundness of the hole are given. The laser was set to a repetition rate of 10, 30 and 90 kHz, with energies between 30 and 80 µJ. However the best quality was obtained with 10 kHz so only results with the repetition rate are presented.

The laser beam was guided with a set of 4 mirrors into the trepanning head in the vertical position. We checked the vertical orthogonality of the laser beam at the end of the optical beam line before injecting it into the trepanning head. Then we made sure to align the laser beam along the optical axis of the head components.

The motorized trepanning head (model Type 3) has been provided by Laser-und Medizin-Technologie Berlin (LMTB) [23]. This Type 3 head has a separate controlling unit which enables the operator to dynamically adjust the current position of the optical elements inside the head. The optical unit is made up of a plane-parallel plate and a variably adjustable wedge plate. This unit is rotated by a drive motor to enable a circular path shaped deflection of the beam. The motor speed is continuously adjustable from 500 rpm to 10,000 rpm. In order to minimize vibration in the head the speed was set to 2,600 rpm. With this setup, we have the possibility to independently adjust the hole diameter and the inclination angle of the rotated beam. This way the head enables to drill cylindrical bore holes and also positive and negatively tapered holes. The focusing unit has a vibration decoupled mounting and is equipped with a lens of 100mm focal length. Details of the head are given in [23]. A gentle flow of Argon across the surface was applied as a shielding gas.

Additional samples of drilled holes have been provided by GFH GmbH. These samples were drilled with GFH's trepanning system "GL.trepan". The system bases on a high rotating and fine balanced precision spindle, which contains a telescope of cylindrical lenses. The diameter and the taper of the hole can be automatically adjusted by controlling the position and the angle of the telescope's input beam with two cnc driven mirrors. The optical setup guides the focussed beam on the working piece with the desired diameter and taper and additionally forces the beam to rotate its profile. The optical rotation speed can be set continously up to 30'000rpm. Pressurized air was used as processing gas. The laser source for drilling the samples was a Trumpf picosecond laser with 1030nm. The laser operated at a fixed repetition rate of 200 kHz with pulse energies between 150 µJ and 250 µJ.

The two drilling setups were run under different parameter sets like rotation speed and repetition rate, which do not allow a direct comparison of processing results. The intention of this publication is merely to evaluate the hole quality of ultrashort pulsed lasers in terms of recast layer and surface roughness than to compare the laser sources or trepanning heads.

2.2 Sample preparation

The material selected for experiments is AISI 440C (pre-hardened and tempered). This stainless steel is commonly used in automotive industries for the fabrication of fuel injectors since it combines its high hardness and good resistance to chemical corrosion. Samples to be drilled are cut by wire-EDM from a cylindrical bar with the thickness of 300 µm and 700 µm, to avoid the occurrence of residual stress. The samples were mounted on controlled X-Y-Z motorized translational stages (AEROTECH pro series) under the trepanning head.

After laser drilling samples are cross-sectioned along the hole axis to analyze the generated inner surface. Cross sections are obtained by a preliminary milling process and consequently finished with a rotating grinder. This operation is carried out under a stereo microscope (maximum magnification 100x) in order to identify the position of microhole as well as the presence of residuals (burrs or contamination). Residuals of the preparation process are removed during a final step of ultrasonic cleaning in ethanol (20min). Hole cross-sections are then analyzed by using Scanning Electron Microscopy (SEM) to visualize the generated surface texture and to characterize the geometrical features along the hole axis. Finally, SEM is used as a cross check measurement of a different imaging technique to afford the robustness of the measuring equipment.

2.3 Experimental procedure

We tried different drilling strategies during the tests, in order to avoid heat affected zone, burrs and uneven edges. We fixed the diameter of each hole between 100 and 200µm at the exit side. The aim was to reach a perfect round and cylindrical hole, or a negative tapered hole. At first we drilled focalizing the beam at the top surface of the material. In a second attempt we drilled focalizing the beam 300µm inside the material in order to be more efficient in the ablation. We also tried moving the Z position in a continuous way through the hole during drilling to the bottom side of the material.

At the end, we tried an alternative strategy separating the process in two steps: first, creating a small hole of the size of the focalized beam by percussion drilling, and then enlarging the diameter by moving automatically the plan parallel plate of the trepanning system, which allowed us a better evacuation of the heat, in order to minimize the heat effects and ameliorate the shape and the edges.

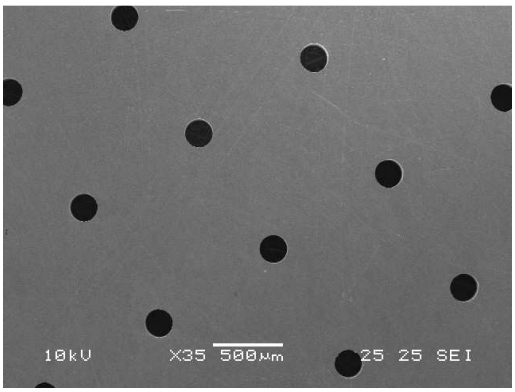

Figure 2: Bottom side of drilled test pattern to verify the statistical error in diameter and roundness (GFH).

2.4 Roughness measurements

Nanoimaging and surface roughness analysis on the prepared samples are carried out by a specifically conceived scanning probe method based on the Shear Force Microscopy (SHFM). Since from the introduction of Atomic Force Microscopy (AFM), many instrumental configurations have been proposed and used in order to reconstruct the morphology of micro-machined surfaces with sub-micrometer spatial resolution [24].

Despite of its extremely large sensitivity, which can lead to atomic spatial resolution, two major issues are relevant in practical applications of AFM-based techniques to machined workpieces. The first one deals with the physical size of the probe, typically shaped in the form of a cantilever with a small pyramidal tip at its end. Analysis of curved surfaces, such as those obtained by micro-drilling, is typically cumbersome because of possible undesired collisions between the cantilever and the surface. The second issue is associated with the operation mode of the AFM. Even though non-contact operating modes have been developed based on tapping, i.e., on a periodical modulation of the tip-to-surface distance, intermittent contact occurs leading to probe blunting. The effects of tip wearing, well investigated as one of the most relevant problems in the frame of nanoindentation [25], are clearly detrimental in terms of spatial resolution. On the other hand, the use of ultra-hard tips, e.g., diamond-made, while preventing such artifacts can lead to unwanted surface modifications and scratching [24].

In order to overcome such limitations, a scanning probe microscope based on the shear forces occurring between a sharp tip metal probe (oscillating parallel to the surface) and the surface was designed and applied [26]. The main mechanism responsible for the shear forces in the actual operating conditions of the experiment is related to the viscous behavior of the thin air layer between the tip and the surface. Among the effects of the shear forces, a dramatic damping of the forced oscillation is measured at tip-to-surface distances in the few nanometers range. The setup, schematically shown in figure 3, employs a piezoelectric actuator to force the oscillation and a piezoelectric transducer to measure the oscillation amplitude.

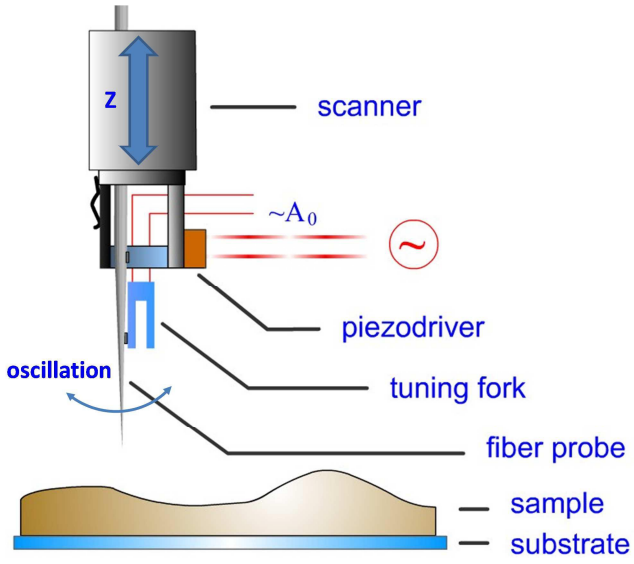

Figure 3. Sketch of the SHFM used in the experiment

In particular, the actuator consists of a PZT layer driven by a sinusoidal signal and able to produce peak-to-peak displacements in the few tens of nm range. The transducer is a quartz tuning fork of the kind typically employed in clock oscillators. A tip, produced by electrochemical etching of a 0.125 mm diameter tungsten wire, is joined to one arm of the tuning fork. The resonance frequency of the tip-tuning fork system is around 33 kHz. The sample is mounted on a three-axis closed-loop nanopositioner (Physik-Instrumente PI.517,3CL) which allows for a maximum travel of 100 μm in the in-plane (x,y) directions and 20 μm in the vertical (z) direction. The nanopositioner is driven by a controller for scanning probe microscopy (RHK SPM 100).

The SHFM approach enables significant advantages if compared to conventional AFM. The length of the tip can be in fact made large enough (0.2-0.5 mm) to penetrate into the specimen under investigation without suffering any mechanical interference. Moreover, since shear forces are used, true non-contact operation is achieved, ruling out any effect due to tip wear. Surface morphology is reconstructed by keeping constant the oscillation amplitude to a predefined value, a fraction of the free-oscillation amplitude, thus ensuring that the tip-to-sample distance is constant at a few nm value during the whole sample scan. To this aim, the oscillation amplitude is continuously monitored and used to drive a feedback circuit which acts on the vertical (z) displacement of the piezoelectric nanopositioner. The SHFM reconstructs the topography map of a sample as a h(x,y) matrix, obtained while scanning the sample in a raster path. Typically, the matrix consists of 256x256 points.

The spatial in-plane resolution depends mostly on the tip size. For the maps presented here, where large size scans are considered, it can be evaluated in a range between tens and hundreds of nanometers. The vertical (z) resolution, affected by the oscillation amplitude measurement accuracy and by **the sensitivity of the nanopositioner, can be less than 10 nm.**

The laser-drilled hole is analyzed in three different areas (50µmx50µm), as reported in Fig. 4: one close to drill starting point (entrance area), one in the center (central area), and the third one at the end of the hole (exit area, where the drilling process ends). In all maps, the row by row raster scan starts from the top and progresses slowly toward the bottom. The sample is mounted in order for the rows to be orthogonal with respect to the hole main axis.

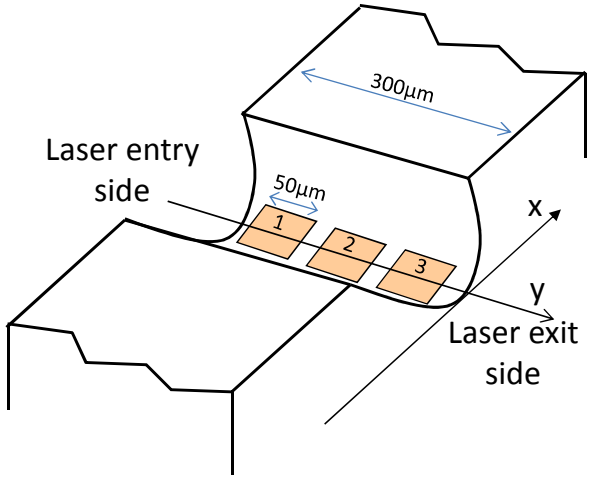

Figure 4. Different investigated areas of the sample: the entrance area (1), central area (2) and the exit area (3).

To measure the surface texture inside a semi-cylindrical hole, the global curvature due to the circular shape of the hole has to be removed. Taking into account that the global curvature is uniform throughout the hole, the curvature is evaluated through best fitting data to a two-dimensional parabolic function by using an image manipulation software [27], and removed from the whole map in order to obtain the topography surface projected over a flat plane. The color palette is then readjusted between the minimum (set now to zero) and the maximum height.

2.5 Metallurgical Analysis

A further analysis practiced on the cut samples is chemical etching to check the presence of a melt layer on the inner wall of the laser drilled hole. At this purpose, samples cross sections are included in thermoplastic resin and prepared for metallurgical analysis by chemical attack with Adler etching. This practice commonly adopted to detect recast layer in case of EDM drilled holes did not reveal on the inner wall metallurgical structures which differ from the base material. It is worth mentioning that the impossibility to notice a uniform melt layer on the machined surface does not imply the total absence of liquid phase formation during laser drilling as it is reported in SEM pictures in the following paragraphs.

3. RESULTS AND DISCUSSION

The combination of complex trepanning system together with femtosecond pulses promises very high precision machining in both geometrical accuracy and surface finish. However at the same time it imposes various pitfalls which are discussed separately in the following sections. First we analyzed the geometrical aspects of the holes in terms of

roundness, taper, entrance and exit edge quality and potential micro cracks. Then in the second section the explicit surface topology and roughness has been examined in different sections of the bore as it is of crucial importance for fluid dynamics of high pressure nozzles. As a general trend we obtained high quality holes with both setups even though the laser parameters in terms of repetition rate were quite different. A significant part of the know how to drill a high quality hole is attributed to the proper process strategy to produce to requested hole geometry in first place and a smooth surface finish at the same time.

3.1 Hole geometry

In order to verify the stability of the process and afford the repeatability of the drilling technique a sample is processed to obtain a matrix of 10 by 10 holes with a spacing of 1mm from each other, see Fig 2. The holes are set to a diameter of 175µm, as depicted in the SEM top view in Fig. 5. Laser parameters and focalization are invariant for each hole so that the tolerance can be evaluated. Measurements of the entrance and exit diameter reveal a standard deviation of about 3% in hole diameter and less than 3% in taper angle. The roundness of the hole on both sides shows deviations of less than 2 µm, which is well within the demands of the automotive industry.

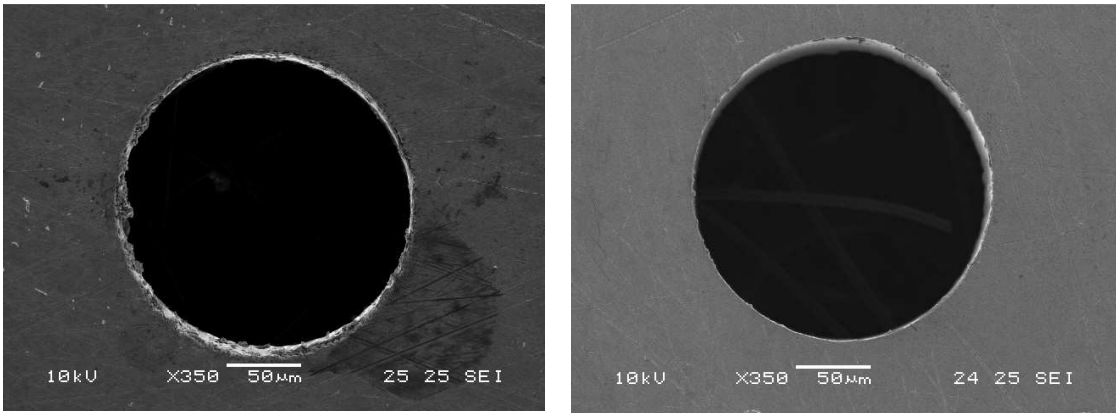

Figure 5: Entrance side (left) and exit (right).of cylindrical hole of 175µm with a tolerance of less than 3% (GFH).

The exit side of the laser beam exhibits better edge quality than the laser entrance side (see Fig. 6). It can be attributed to the shorter exposure time with the laser light. This effect is sometimes referred to as "light in shadow": As the peak intensity is above the ablation threshold by at least one order of magnitude, the energy in the side wings of the beam profiles is sufficient to ablate the rim of the entrance by direct vaporization and by melt creation. This leads to a gentle rounding of the contour with some distinct groves caused by striation. As the effects only occur on the entrance side of the laser, which is typically the exit side of the gas stream on an injection nozzle, it can be tolerated. No micro cracks have been found during the investigations, which supports the finding of the metallurgical analysis, that the heat affected zone can be neglected see 2.5).

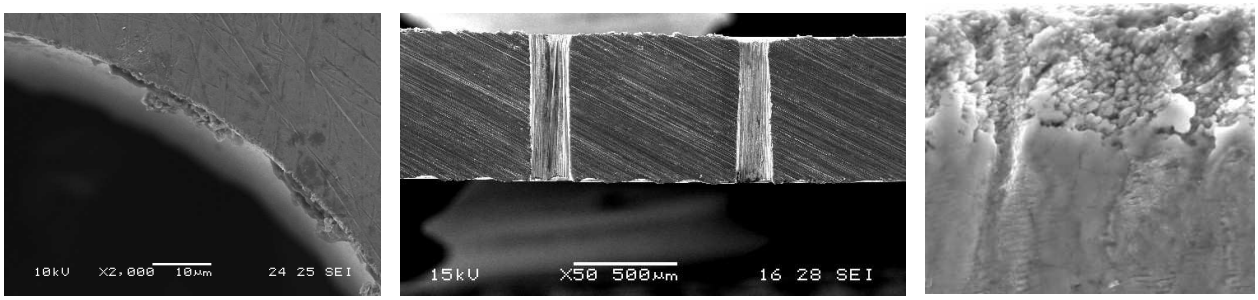

Figure 6: Cross section of a cylindrical hole and a negative taper hole (middle) in 700µm stainless steel (LMTB head). Closeups of the edges show high edge quality, no burr or recast layers can be found. On the left a roughened rim of the entrance side can be seen (GFH,closeup of Fig 5b). On the right (close-up of Fig 13a, GFH) the high magnification shows a distinct topography as discussed in the section 3.3.

3.2 Deviations from the optimal shape

During the installation and alignment of the femtosecond laser and the LMTB head various defects in the hole geometry occurred which can be traced back to optical effects of the beam guidance setup. Great care has to be taken on the optical path to obtain full control of the beam profile along the propagation of the laser beam from entry to exit of the machined sample. Optical components like mirrors lenses beam expanders and prisms introduce astigmatism and change of polarization. Non-linear crystals for frequency conversion can lead to wavefront distortions along their different birefringent axis leading to astigmatism. If astigmatism is not compensated the two directions of polarization have different focal positions. This leads to elliptical focus spots with a rotation of the ellipse orientation along the z-direction.

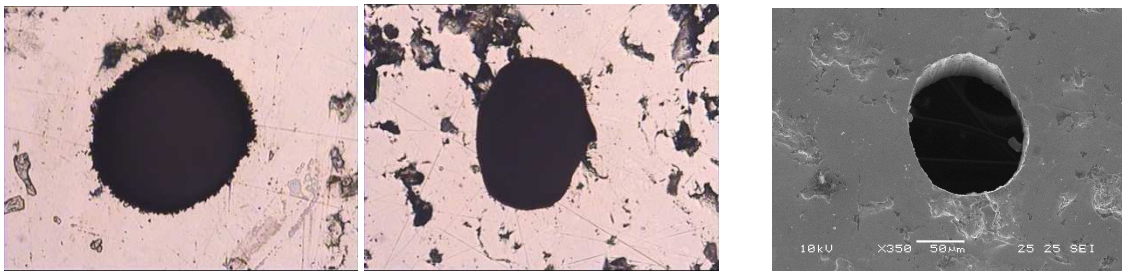

Figure 7: Microscope images of front and backside (left) of an asymmetric hole due to astigmatism, SEM view of same hole on the right

Drilling with such an uncompensated optical setup provides holes with round entrance and elliptic exit or even ellipses on both sides with rotating axis as can be seen in Fig 7. The SEM picture in the projection of 45° gives an insight of the change in beam profile along the propagation.

Therefore it is crucial to have 3D focus spot analysis prior to the installation of the trepanning head to prevent from irregular hole geometries.

3.3 Surface morphology

SEM images of cross sections of GFH samples have been taken and analysed in detail. They show a quite uniform surface texture (excluding entrance and exit edges) in which only slight striations are visible. This testifies that the removal process takes place mostly by pure ablation and a limited liquid phase is spread out along the hole thickness by the motion of the beam.

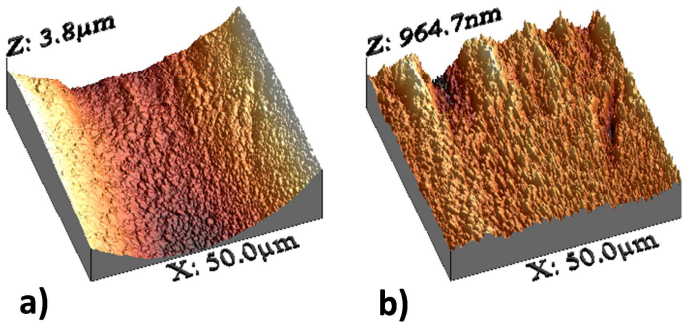

Figure 8: Topography map of the entrance area of the hole: (a) pseudo 3D topography (b) pseudo 3D topography after parabolic filtering to remove the hole curvature.

Similar results can be derived by the SHFM which enables drawing topography maps of the whole scanned area shown in Fig. 8. As reported in 2.4, the curvature (present in Fig. 8.a) of the hole has to be removed by the software in order to obtain a flat surface (Fig. 8.b) on which it is possible to measure the real roughness and waviness of the surface. This

reveals a maximum peak to valley distance of 965 nm, with a major waviness on the entrance and a much smoother surface after the first 25 µm inside the hole. The different sections of the hole are investigated in more detail below.

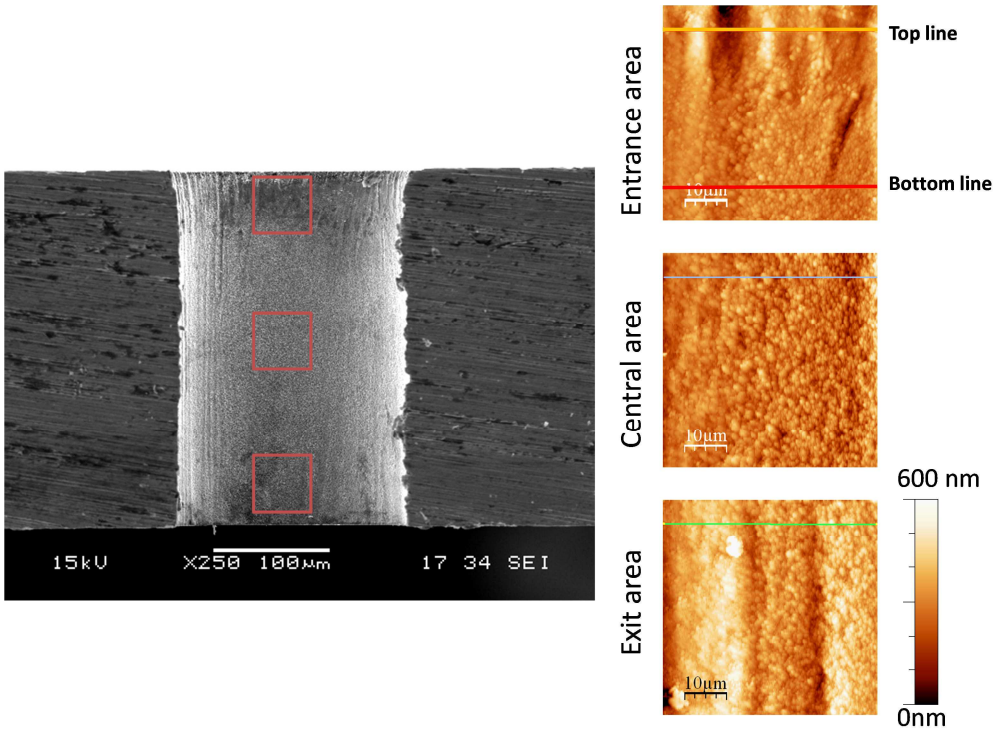

Figure 9: SHFM topography maps in the three areas

Fig. 9 illustrates the evolution of the topography maps (squared areas with 50µm side and resolution 256x256) along the hole axis. For each map the darkest point represents the deepest valley, conversely the lightest one is the highest peak (relative maximum excursion in z of 600nm). It is worth mentioning that since SHFM sets to zero the deepest point of each map, the absolute value of the height is not homogeneous for the three areas. Striations can be noted (darkest longitudinal areas) in all the three maps: as a result the surface structure seems to be based on the superposition of a larger texture axially developed and secondary one with lower amplitude and higher frequency.

It can be also noted that the entrance area shows the higher waviness of the surface at the upper edge related with an excess of heat accumulation, also visible in SEM images. To quantify the entity of this waviness which differs from the quite uniform inner surface, line profiles (perpendicular to the hole axis) can be extracted from the topography map. The orange line profile in figure 10 represents the waviness of the entrance edge with a period of about 15µm, while the red one is taken in a more uniform zone which represents the common aspect of the whole surface.

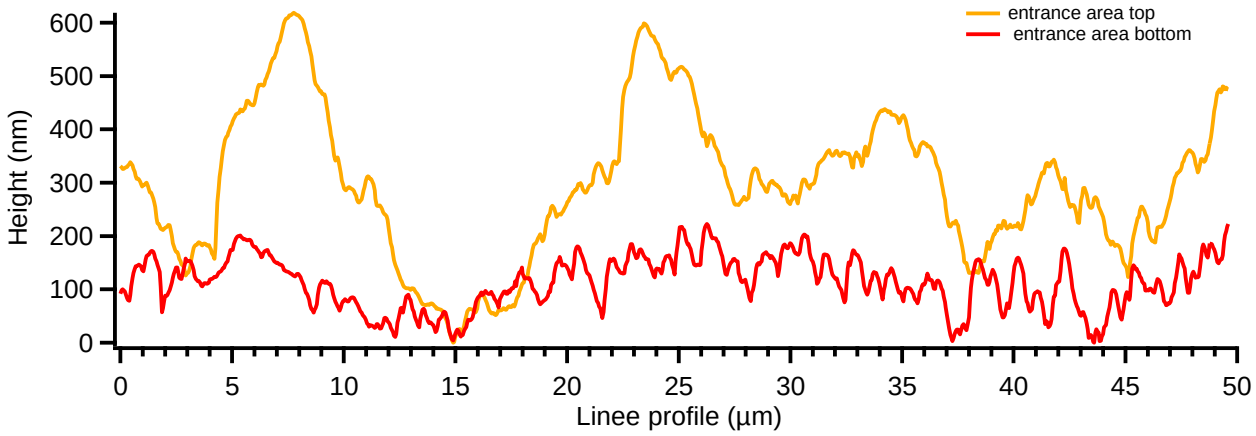

Figure 10: Two different line profiles on the entrance area reported in Fig.9: top line and bottom line.

In figure 11 line profiles for the three maps are reported together: taking into account that the zero value is not the same for the three maps, only measurements on the distance between maximum peak and minimum valley (globally in the range of 0-300nm) can be properly derived. If we exclude the entrance edge, the occurrence of peaks and valley is quite uniform for different positions in the material thickness thus demonstrating the uniformity of the material removal process.

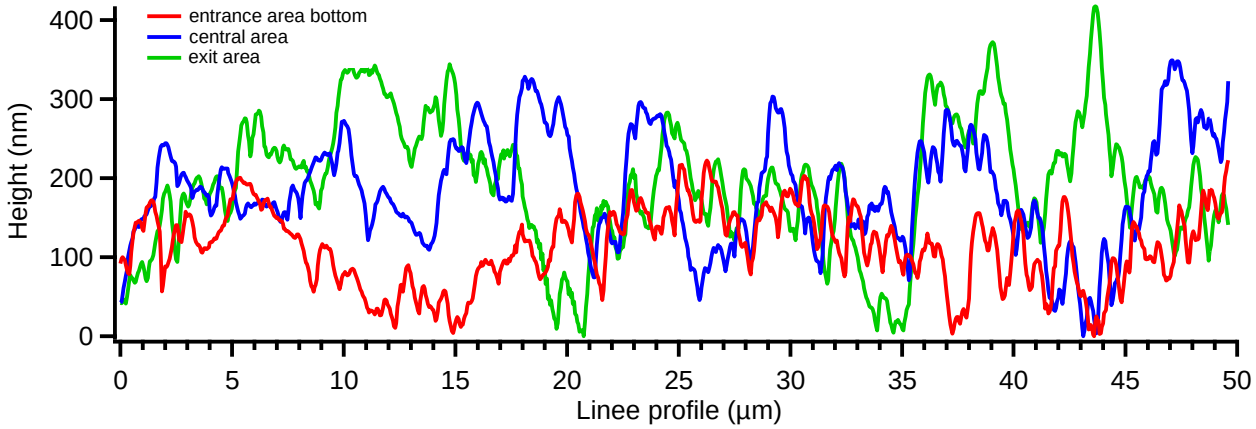

Figure 11: Line profiles in the three areas, colors are referred to the lines reported in fig.4.

To analyze the effect of the laser drilling process on surface roughness, the acquired SHFM maps are analyzed by the root-mean-square surface roughness, R_Q [28]. The graph in figure 12 shows the calculated R_Q over the 256 rows (y direction in Fig.4) for each scanned area. As a result the graph points out the R_Q behavior on a total distance of 150µm along the hole axis: at the entry edge the roughness is affected by waviness described above giving maximum values of 160nm. In a central zone reaches its minimum averaged value of 67nm, then it increases again. Being the total excursion of measured height of the exit area similar to the previous two (see Fig. 11) the higher deviation from the least squared line in Fig. 12 can be explained by the accumulation of the thin melt layer in correspondence of the exit edge of the laser. This means that surface roughness cannot be retained constant in every position during the drilling process.

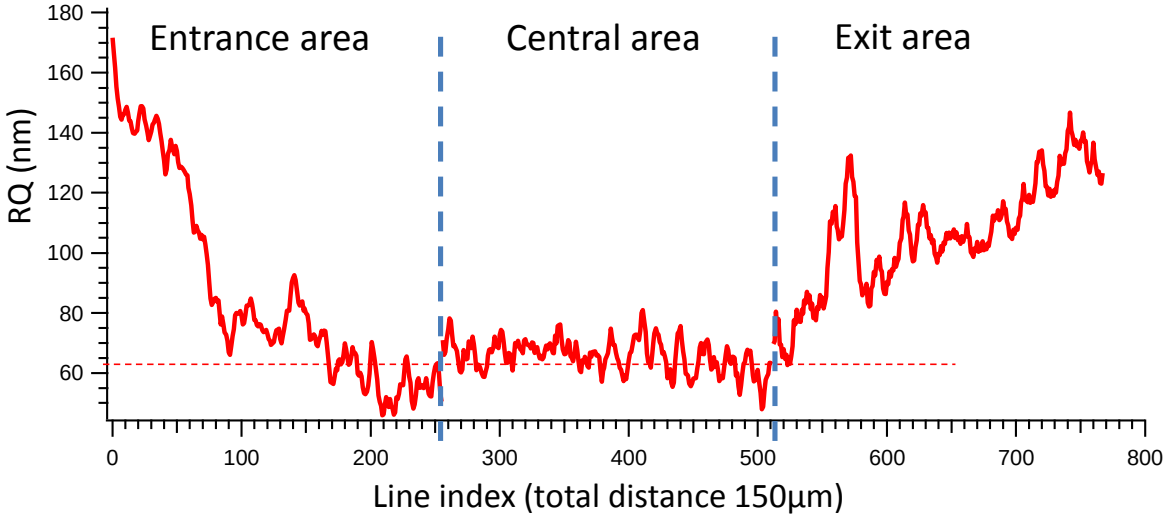

Figure 12: Evolution of root-mean-square surface roughness inside the laser drilled hole.

It is well known in the literature that roughness on surfaces generated by an orthogonal ultrashort-pulsed laser is related to the formation of periodic structures, namely Laser Induced Periodic Surface Structures LIPSS. In the actual case the presence of such structures is clearly visible at the entrance area with clear and uniform periodic structures depicted and measured in Fig. 13.

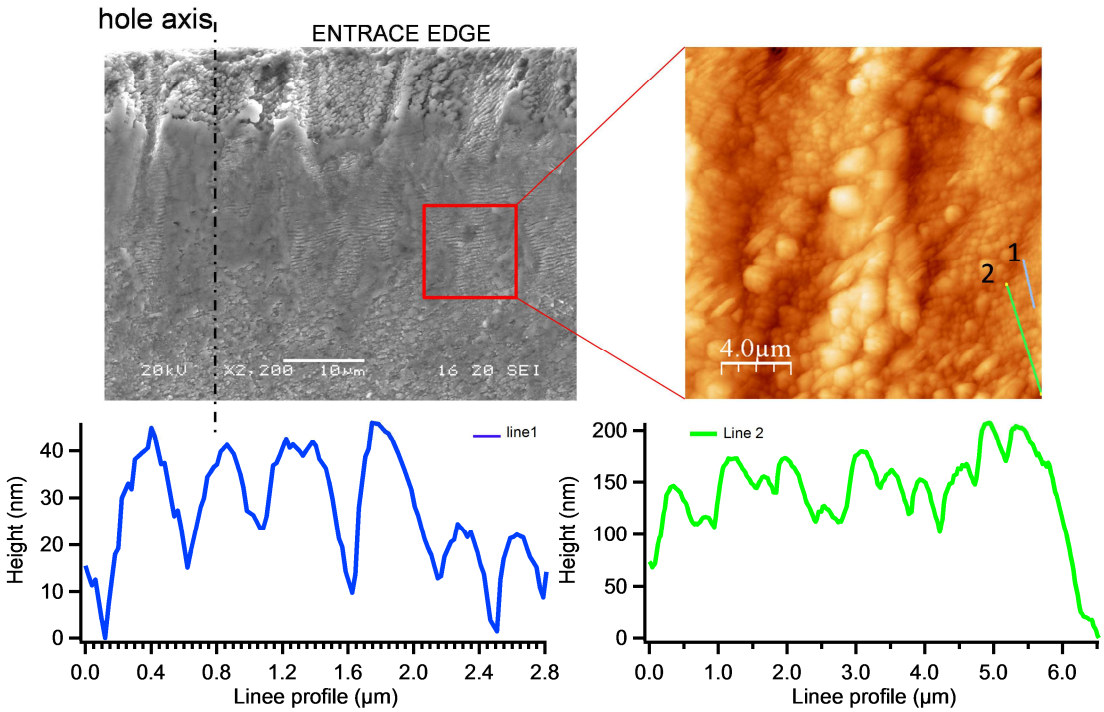

Figure 13: Formation of Laser Induced Periodic Surface Structures (LIPSS) at the entrance area and their measurement with SHFM.

A magnification of the entrance area shows that between consecutive striations (darkest longitudinal areas) it possible to notice low spatial frequency LIPSS (LSFL) with a period of about 500nm and a total height, measured for line 1 and 2 in Fig.13, ranging between 50-200nm.

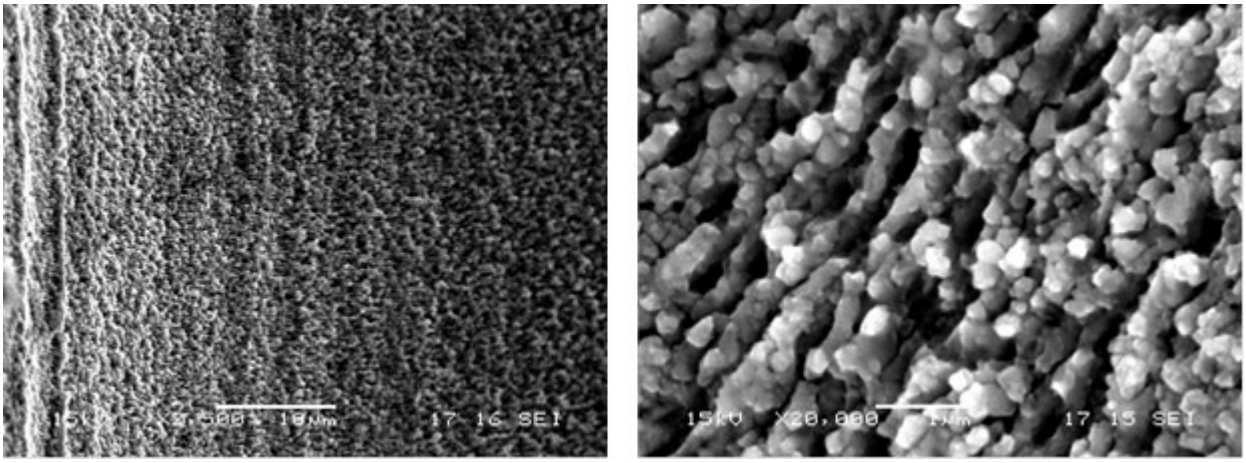

Figure 14: Formation of Laser Induced Periodic Surface Structures (LIPSS) at the central at SEM and their magnification.

LIPSS structures evolve along the thickness of the sample depending on the fluence adopted and the irradiation time. According to [29] the expansion of high energy irradiated material is subjected to violent solid-gas transition in his upper layer and part to melting (solid-liquid) or phase explosion (liquid-gas) in deeper layers. This might be the cause of breaking the periodicity of the structures formed on the entrance area.

4. CONCLUSIONS

Drilling of holes with full control of the 3D shape able to meet restrictive industrial specifications is a very challenging task. It was shown that ultrashort pulsed lasers in combination with trepanning optics offer a promising solution to these high demands when all input parameters are under full control. The capabilities of the laser setup to drill microholes of repeatable diameter with a negligible heat damage on the inner surface was tested by means of Shear Force Microscopy SHFM. Its application on complex (curved) shapes represents a novelty even in the field of nanoscale surface inspection. The possibility to use a direct measurement of peaks and valleys (with respect to indirect measurements based on light refraction) can be retained a step towards the standardization of the surface structures inside the holes (e.g. Ra, Rq parameters).

Measurements carried out on laser drilled holes realized during the research activity show a remarkable improvement of surface quality with respect to the traditional EDM process. The root-mean-square surface roughness is globally measured around 60-100nm while the entrance side reveals higher values due to the superposition of a primary waviness, whereas the EDM process typically provides surface roughness of 300nm. As a result holes drilled with the experimental setup described offer a smooth surface along the thickness of the sample combined with an extremely sharp edge at the exit side. These two characteristics should make ultrashort laser processing a very interesting tool for the automotive industries aiming for highly atomized spray jets.

ACKNOWLEDGEMENTS

We would like to gratefully thank Amplitude Laser Systems for providing the high power Femtosecond laser as well as GFH GmbH for their collaboration in demonstrating their drilling system and drilling samples accordingly. We also acknowledge the LMTB Berlin for supplying the trepanning head and the Region of Aquitaine for the funding of this research.

REFERENCES

[1] Chichkov B N, Momma C, Nolte S, von Alvensleben F, Tünnermann A 1996 Appl. Phys. A 63 109
[2] Preuss S, Demchuk A, Stuke M 1995 Appl. Phys. A 61 33
[3] Zhu X, Naumov A Yu, Villeneuve D M, Corkum P B 1999 Appl. Phys. A 69 S367
[4] Shirk M D, Molian P A 1998 J. Laser Appl. 10 1
[5] Nolte S, Momma C, Jacobs H, Tünnermann A, Chichkov B N, Wellegehausen B, Welling H 1997 J. Opt. Soc. B 14 2716
[6] Wellershoff S S, Hohlfeld J, G¨udde J, Matthias E 1999 Appl. Phys. A 69 S99
[7] Furusawa K, Takahashi K, Kumagai H, Midorikawa K, Obara M 1999 Appl. Phys. A 69 S359
[8] Zhigilei L V 2003 Appl. Phys. A 76 339
[9] Banks P S, Feit M D, Rubenchik A M, Stuart B C, Perry M D 1999 Appl. Phys. A 69 377
[10] Wynne A E, Stuart B C 2003 Appl. Phys. A 76 373
[11] Klein-Wiele J-H, Marowsky G, Simon P 1999 Appl. Phys. A 69 S187
[12] Nishikawa H, Kanai M, Szabo G, Kawai T 2000 Phys. Rev. B 61 967
[13] Bonse J, Baudach S, Kautek J, Lenzner M 2002 Appl. Phys. A 74 19
[14] Gamaly E G, Rode A V, Tikhonchuk V T, Luther-Davies B 2002 Appl. Surf. Sci. 8094 1
[15] Perez D, Lewis L 2003 Phys. Rev. B 67 184102
[16] Schäfer C, Urbassek H M, Zhigilei L V 2002 Phys. Rev. B 66 115404
[17] Anisimov S I, Inogamov N A, Oparin A M, Rethfeld B, Yabe T, Ogawa M, Fortov V E 1999 Appl. Phys. A 69 617
[18] Y. L. Yao, H. L. Chen and W. Zhang, (2005), "Time scale effects in laser material removal: A review." The International Journal of Advanced Manufacturing Technology, 26 (5), Page 598-608.
[19] Lin Li, C. Diver, J. Atkinson, R. Giedl-Wagner and H.J. Helml, “Sequential laser and EDM Micro-drilling for next generation fuel injection nozzle manufacture”, Annals of the CIRP, Manufacturing Technology, Vol. 55, No.1, 2006, pp.179-182
[20] S. I. Anisimov, B. L. Kapeliovich, and T. L. Perel’man, in: Sov. Phys. JETP 39, 375, 1974.
[21] Z. Lin, L.V. Zhigilei, V. Celli, Phys. Rev. B 77, 075133 (2008)
[22] Mielke, M. M., Booth, T., Greenberg, M., Gaudiosi, D. M., Martinez, C., Sapers, S. P., Cline, R., et al. (2012). Applications of Ultrafast Lasers in Microfabrication. LMP 2012 (pp. 1–8).
[23] Ashkenasi, D., Mueller, N., Kaszemeikat, T., Illing,. (2010). Advanced laser micro machining using a novel trepanning system. Proceedings of *LPM2010* (pp. 1–5)
[24] For a review, see for instance: B. Bhushan (Ed.), Springer Handbook of Nanotechnology, 3rd edition (Springer-Verlag, Heidelberg New York, 2010)
[25] M. Alderighi, V. Ierardi, F. Fuso, M. Allegrini, R. Solaro, Size effects in nanoindentation of hard and soft surfaces, Nanotechnology 20 (2009), pp. 235703-1-9
[26] K. Karrai, I. Tiemann, Interfacial shear force microscopy, Physical Review B, 62(19) (2000), pp 13174-13181
[27] I. Horcas, R. Fernandez, J.M. Gomez-Rodriguez, J. Colchero, J. Gomez-Herrero, A.M. Baro, WSxM: a software for scanning probe microscopy and a tool for nanotechnology, Rev. Sci. Instrum. 78 (2007), 013705
[28] Degarmo, E. Paul; Black, J T.; Kohser, Ronald A. (2003), Materials and Processes in Manufacturing (9th ed.), Wiley, p. 223
[29] Vincenc Obona J., Ocelìk V., Skolski J.Z.P., Mitko V.S., Römer G.R.B.E., Huis in’t Veld A.J., De Hosson J.Th.M., 2011, On the surface topography of ultrashort laser pulse treated steel surfaces, Applied Surface Science, 258, pp. 1555-1560
[30] G. Cusanelli , M. Minello , F. Torchia , W. Ammann and P.-E. Grize "Properties of micro-holes for nozzle by micro-EDM", *Proc. 15th Int. Symp. Electromach. (ISEM XV),* pp.241 -245 (2007)